Effect of the Linking Group on the Thermoelectric Properties of Poly(Schiff Base)s and Their Metallopolymers

Jiahua Li,[a,b] Zitong Wang,[a] Zelin Sun,[b] Linli Xu[a,b] and Wai-Yeung Wong*[a,b]

[a] Jiahua Li, Zitong Wang, Dr. Linli Xu, Prof. Wai-Yeung Wong
Department of Applied Biology and Chemical Technology and Research Institute for Smart Energy
The Hong Kong Polytechnic University
Hung Hom, Kowloon, Hong Kong (P. R. China)
E-mail: wai-yeung.wong@polyu.edu.hk

[b] Jiahua Li, Dr. Zelin Sun, Dr. Linli Xu, Prof. Wai-Yeung Wong
The Hong Kong Polytechnic University Shenzhen Research Institute
Shenzhen 518057 (P. R. China)

Abstract: As the polymer-based thermoelectric (TE) materials are highlighted by their attractive features such as light weight, flexibility, low toxicity and ease of processibility, an increasing number of conducting polymers and their composites with high TE performances have been developed in recent years. Up to date, however, the research focusing on the structure–performance relationship remains rare. In this paper, two series of poly(Schiff base)s with either C=C or C≡C linker and their metallopolymers were synthesized and doped with single-walled carbon nanotubes to evaluate how the linking groups affected the TE properties of the resulting composites. Apart from the effect exerted by the morphology, experimental results suggested that the linkers played a key role in determining the band gaps, preferred molecular conformation and extent of conjugation of the polymers, which became key factors that influenced the TE properties of the resulting materials. Additionally, upon coordination with transition metal ions, the TE properties could be tuned readily.

Introduction

Thermal power generation, as the dominant approach by far, provides the vast majority of electrical energy for our daily life. However, during this process, more than half of the energy is dissipated in the form of heat which is regrettably released to the air afterwards.[1] Emerging as a clean power generation solution, thermoelectric (TE) materials realize the conversion between heat and electricity, and thus have attracted increasing research interest in recent years. The conversion efficiency of a TE material is influenced by its electrical conductivity (σ, $S \cdot m^{-1}$), Seebeck coefficient (S, $V \cdot K^{-1}$), thermal conductivity (κ, $W \cdot m^{-1} \cdot K^{-1}$) and testing temperature (T, K) and is assessed by their product – a dimensionless parameter named figure-of-merit (ZT) which is defined as: $ZT = S^2\sigma T\kappa^{-1}$. Therefore, materials with high σ and S, but low κ are desirable. So far, some inorganics have been demonstrated to show superior efficiency with ZT > 1.0, represented by Bi-Te-based alloys,[2] lead chalcogenide[3] and SiGe.[4] Nevertheless, their applications are quite restricted, as these materials are generally hard to be processed and heavy or rare metal elements are always included.[1c, 5]

By contrast, organic TE (OTE) polymers are generally featured with light weight, low toxicity, low κ, good flexibility, variable structures and ease of processing,[1c, 5-6] and thus have shown promising potential in niche applications such as room temperature coolers, mini power generators and especially the devices that contact human body directly.[1a, 1b, 7] In view of the low thermal conductivity of OTE polymers, power factor (*PF*) is preferred to evaluate the TE performance of these materials, where $PF = S^2\sigma$.[5a, 8] With conjugated main chains acting as the structural characteristic, a number of polymer-based TE materials have been developed. However, other than some classical structures including poly(3,4-ethylenedioxythiophene) : poly(styrenesulfonate) (PEDOT:PSS),[9] poly(3-hexylthiophene) (P3HT),[10] 1,1,2,2-ethenetetrathiolate-based metallopolymers (poly(M-ett)),[11] etc., most pure OTE polymers still suffer from low TE performances[12] and remain to be explored. As an effective solution, doping has been widely applied to significantly enhance the electrical conductivity and the TE performance.[13] Among the commonly used conductive nanofillers, carbon nanotubes (CNTs) attracted the most intense research interest because of their excellent electrical conductance, high charge carrier mobility and mechanical properties.[14] For example, the *PF* of polypyrrole was dramatically boosted up to over 300 times after SWCNTs were introduced.[15] In light of the advantages of SWCNT-based doping, a detailed comparison between two blending approaches (i.e. the *in situ* preparation and physical mixing) were made to check the difference in TE performance of a poly(Schiff base)-SWCNT composite system.[16] The composites prepared in the physical mixing fashion were demonstrated to yield higher *PF* with the top value of 77.7 ± 5.8 $\mu W \cdot m^{-1} \cdot K^{-2}$ at a polymer/SWCNT ratio of 1/3.[16]

Furthermore, a few underlying studies looked into the relationship between molecular structures and the TE properties from various aspects. For example, it was found that the heteroatoms in the poly(3-alkylchalcogenophene) system played a key role in determining the TE properties.[17] The enhanced electrical conductivity but weakened thermal power can be observed by altering the chalcogen atoms from S to Se to Te. By merging thiophene and carbazole moieties into the poly((9,9-dioctylfluorene)-2,7-diyl-*alt*-benzothiadiazole) structure, the polymers were demonstrated to exhibit optimized TE properties with the peak *PF* value of 13.11 $\mu W \cdot m^{-1} \cdot K^{-2}$ at 90 °C.[18] In addition, some studies investigated the roles of side chains played in determining the TE properties of polymer-based OTE materials.[19]

There is no doubt that the way how functional units are organized is another critical factor that determines the physical properties of a polymer material. Hence, once the functional fragments have been decided, it is feasible to tune the

performance of polymers by integrating those segments with various linkers. However, to the best of our knowledge, relevant research is still rare.

In light of the ease of synthesis and the potential coordination capability, in this work, we selected poly(Schiff base) as the model and fully addressed how the linking groups affected the TE properties by comparing two structurally resembled 1,4-diazabuta-1,3-diene (DAB)-linked poly(Schiff base)-SWCNT composite systems. As for the poly(Schiff base)s (i.e. **P1** and **P2** shown in Scheme 1), similar main chains were built by employing *trans*-stilbene and diphenylacetylene structures to bond with the adjacent DAB fragments, so that the difference in performance could be ascribed to the effects due to the linker type (C=C versus C≡C). The polymers were synthesized through condensation polymerization and the composites with stepwisely increased SWCNT mass contents [f_C, f_C = ($m_{SWCNT}/m_{composite}$)×100%] were prepared. The TE properties of the formed composites were studied and further tuned by incorporating various transition metal ions (Co^{2+}, Ni^{2+} and Cu^{2+}) to the DAB sections. Based on the performance assessment, the effects of the linking groups on the TE properties were discussed from the perspective of band structures, molecular conformations and the contact modes between the polymer chains and the SWCNT networks.

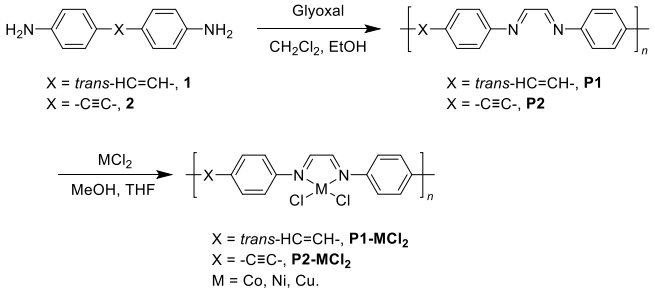

Scheme 1. Synthetic route of polymers **P1** and **P2** and their metallated products **P1-MCl₂** and **P2-MCl₂**.

Results and Discussion

Chemical structure determination

Considering the highly conjugated chain structures and the resulting rigid molecular backbones, all these polymers are hardly soluble in common organic solvents, and hence the attempts by using nuclear magnetic resonance spectroscopy to determine the structures were impractical. Therefore, the chemical structures of the polymers were identified by Fourier-transform infrared (FTIR) spectroscopy. As shown in Figure 1, the aligned absorption bands at 960 cm^{-1} was induced by the bending vibration of the disubstituted C=C bond, suggesting that the linker in **P1** and **P1-MCl₂** was in a *trans*-configuration.[20] Specifically, a characteristic absorption band corresponding to the stretching vibration of the imine bond[16] in **P1** was detected at 1679 cm^{-1}, suggesting the successful synthesis of the target polymer. As expected, this band was found to shift to the higher wavenumber region to a different extent after coordination with metal ions. Besides, the strong signals at 831 cm^{-1} is assigned to the C-H vibration on the *p*-disubstituted phenyl rings.[20] By comparison, the FTIR spectra of **P2** and **P2-MCl₂** (Figure S3) displayed similar patterns, in addition to the emergence of a weak absorption band at 2206 cm^{-1} due to the internal C≡C in the polymer chains.[20]

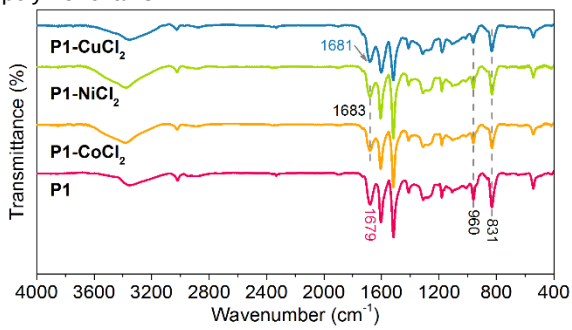

Figure 1. FTIR spectra of **P1** and **P1-MCl₂**.

Morphology study

The microstructure of the as-prepared composite films was investigated by scanning electron microscopy (SEM). As shown in Figure 2, at a low SWCNT doping ratio (f_C = 15%), phase separation behaviour was evidently observed. Nanotube bundles are connected with each other, forming sparse and layered network structures with aggregated **P1** or **P1-MCl₂** particles sitting atop or underneath. Interestingly, the continuous introduction of SWCNT led to a significant morphology evolution. A condensed CNT network was established and some polymer particles began to fuse themselves with it when f_C reached 45%. At this point, it is hard to distinguish the boundaries between one layer of CNT network and its adjacent ones. The interactions among CNTs were dramatically improved and such an effect was additionally enhanced by the coated poly(Schiff base), due to the increased contact area. When the doping ratio f_C climbed up to 90%, a homogeneous and continuous surface was observed without the abrupt appearance of individual particles any longer, implying that all OTE polymers have been well dispersed in the composites. By comparison, a similar morphology change could be found for **P2**-SWCNT and **P2-MCl₂**-SWCNT composite films (Figure S4), except that severe phase separation was still retained even at the medium doping level, which may imply inferior electrical conductivities.

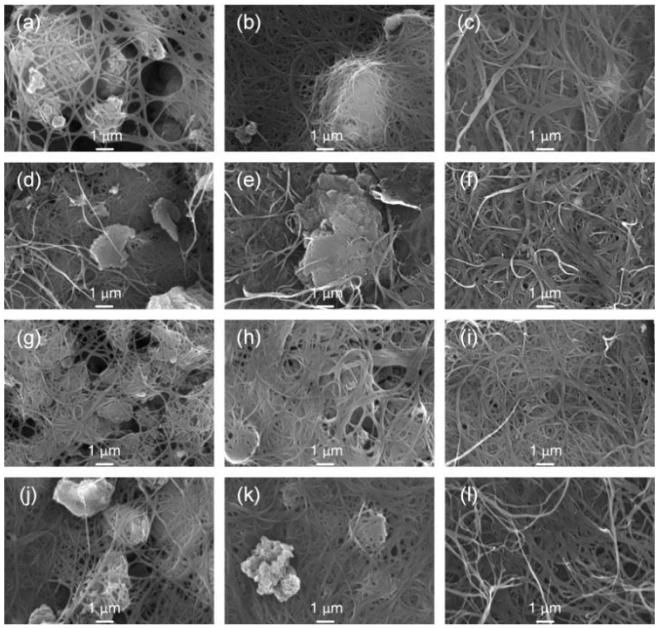

Figure 2. SEM images of the (a-c) **P1**-SWCNT, (d-f) **P1-CoCl$_2$**-SWCNT, (g-i) **P1-NiCl$_2$**-SWCNT and (j-l) **P1-CuCl$_2$**-SWCNT composites films with the doping ratio (f_C) of 15% (left column), 45% (middle column) and 90% (right column).

Raman spectral analysis of the (metallo)polymer-SWCNT composites

Based on the gradual evolution of the morphology, we speculated that the interactions through polymer chains and SWCNT networks may come into play during the blending process. To prove this, Raman spectra were measured (Figures 3 and S5). For pure **P1** powder, two main absorption bands at 1165 and 1562 cm^{-1} were detected, which corresponded to the C-H bending and imino stretching vibrations, respectively.[16] The Raman spectra of the pure SWCNT film was composed of a radial breathing mode (RBM) at 159 cm^{-1}, an out-of-plane bending mode (D band, 1307 cm^{-1}), a characteristic in-plane, anisotropic stretching vibration of bonded sp^2 C atoms (a G$_-$ band at 1571 cm^{-1} and a G$_+$ band at 1592 cm^{-1}) and a 2D band at 2594 cm^{-1}.[21] By comparison, the blending process brought about a blue shift at the G$_+$ band, which not only illustrated the effective π-π interactions between the polymer chains and the SWCNT networks, but also indicated an electron migration route from SWCNTs to the OTE polymer chains, known as a typical p-doping behaviour.[22] Similar spectral profiles and behaviour were detected from **P2** and **P2**-derived composite systems (Figure S5), in addition to the presence of the new peak at 2214 cm^{-1} from neat **P2** which was due to the C≡C stretching.

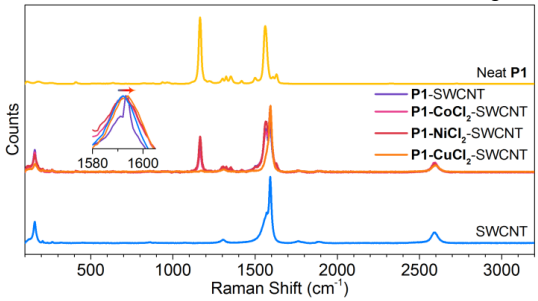

Figure 3. Raman spectra of **P1**, SWCNT, **P1**-SWCNT and **P1-MCl$_2$**-SWCNT composites at f_C = 45% under the excitation by a laser at 785 nm.

TE properties

The TE performances (including the electrical conductivity, Seebeck coefficient and *PF*) of the metallopolymer-SWCNT composites were assessed at RT and are displayed in Figure 4. As can be seen from Figures 4a and 4d, the electrical conductivities of the composites were remarkably enhanced upon the gradual addition of SWCNT. At the lowest SWCNT content, **P2**-SWCNT composite showed a higher σ value than **P1**-SWCNT. This may be benefited from the more uniform morphology: **P2** particles were better dispersed in the mixture and a condensed carbon nanotube network was developed (Figure S4a). Additionally, those polymer particles combined more tightly with the nanotube bundles. Under this circumstance, intermolecular charge carrier transmission via CNTs and polymer chains, especially that among the nanotube bundles in the inter-plane fashion, was significantly promoted and thus a higher conductivity property was endowed. Expectedly, thin films in both series gave their highest electrical conductivity at f_C = 90%, but **P1**-SWCNT composites displayed superior values when the SWCNT content was beyond 45%. Other than the effects brought about by the morphologies, we proposed that such a distinctive phenomenon may stem from the differences in the preferential molecular conformations and the conjugation length, which will be discussed in detail later.

Furthermore, we tried to tune the electrical conductivity of the materials by binding metal ions to the poly(Schiff base) ligands. In the case of **P1-MCl$_2$**, the coordinated Co^{2+} and Ni^{2+} increased the σ value by 26% and 45%, respectively, at f_C = 15%, when compared with their metal-free version. As the metallopolymers were the dominate component at the initial doping ratio, we may describe as well the possible factors mainly from the perspective of conducting metallopolymers. According to previous reports, such an enhancement would probably benefit from the intramolecular redox matching mechanism[23] and the additional interactions between metal centres and the SWCNT.[14a] In terms of molecular structure, metal centres herein are bonded to the conducting main chains directly through a d-π conjugation fashion, which is a typical instance of the Wolf type II conducting metallopolymer. Under such a condition, if redox-active metal centres (Co^{2+} or Ni^{2+}) were involved and their redox potential were close to or matched with that of the organic backbone, the conjugation and the charge carrier migration route could be extended, resulting in an elevated electrical conductivity (Figure 5a). However, the incorporation of redox-inactive Cu^{2+} would not change the charge transfer route, even if the d-π interaction is retained (Figure 5b). Besides, considering the steric hindrance effect brought about by Cu^{2+} and its auxiliary ligand, **P1-CuCl$_2$**-SWCNT exhibited a lower σ than its metal-free analogue. By contrast, **P2-MCl$_2$**-SWCNT failed to yield higher electrical conductivity than **P2**-SWCNT at f_C = 15%, which may result from the redox mismatching consequences. The electrical conductivity of these metallated composites also showed upward trends with the increasing SWCNT content, although the advantages caused by redox matching diminished. This was probably influenced by the gradually homogenized morphology, increased charge carrier mobility, elevated charge carrier concentration, and the continuously improved charge carrier route. The highest σ value of 9.25×10^4 S·m^{-1} was achieved by **P1-NiCl$_2$**-SWCNT composite at f_C = 90%, nearly 20% higher than that of **P1**-SWCNT at the same doping level.

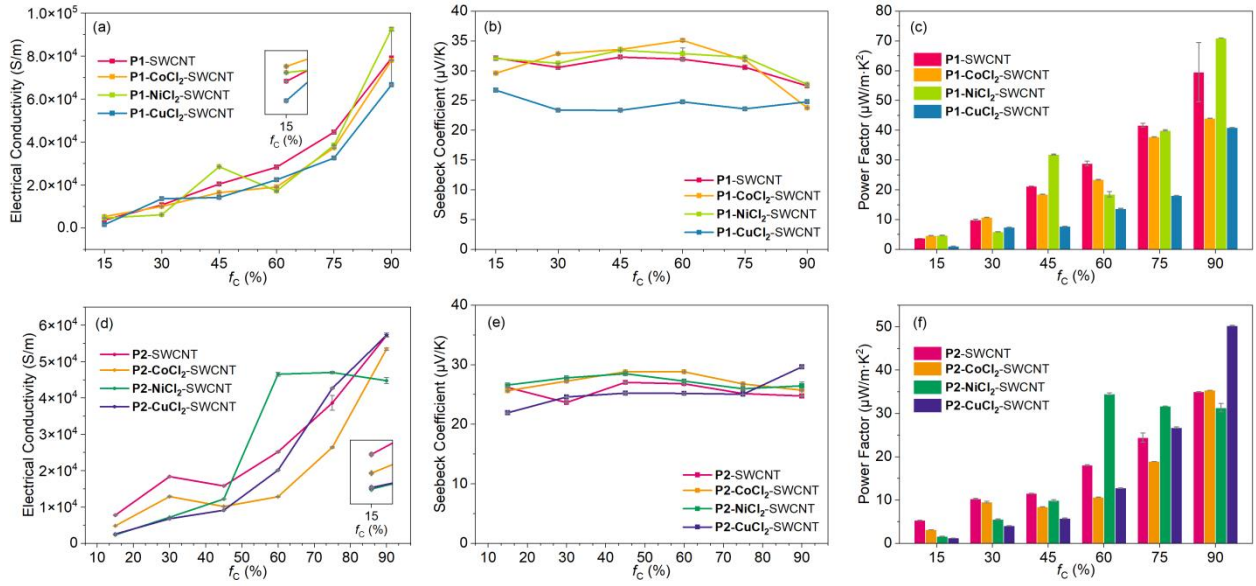

Figure 4. Electrical conductivity, Seebeck coefficient and *PF* of (a-c) **P1**-SWCNT, **P1-MCl$_2$**-SWCNT, (d-f) **P2**-SWCNT and **P2-MCl$_2$**-SWCNT composites at various f_C.

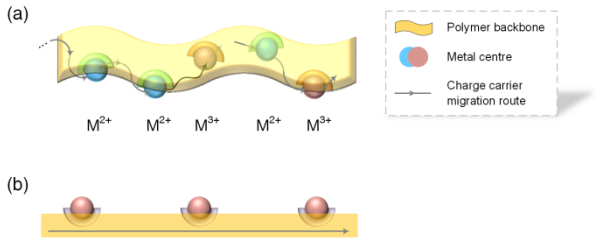

Figure 5. Mechanism of the charge carrier transfer in the Wolf type II conducting metallopolymer, where the orbital energies of the metal ions (a) matched or (b) mismatched that of the polymer chains.

The variation trends of the Seebeck coefficient are displayed in Figures 4b and 4e. All the composites gave positive *S* values, suggesting their p-type semiconducting nature with the holes as the predominant charge carriers. Beyond our expectation, the Seebeck coefficient of these materials did not exhibit a sharp declining trend. Instead, the *S* values in **P1**- and **P2**-derived composites wandered at around 30 and 25 V·K^{-1}, respectively. Such an unusual phenomenon was possibly induced by the energy filtering effect.[24] At the crystallite boundaries, charge carriers with higher energy were selected and allowed to pass by,[24] which possibly cancelled the side effect caused by the elevated electrical conductivity and thus maintained the Seebeck coefficient at a certain level.

Under the combined effects of electrical conductivity and Seebeck coefficient, most **P1**-SWCNT and **P1-MCl$_2$**-SWCNT (M = Co and Ni) composites produced higher *PF*s when f_C exceeded 45%, with the highest record of 71.0 μW·m^{-1}·K^{-2} established by **P1-NiCl$_2$**-SWCNT at f_C = 90% (Figure 4c). The TE properties of the SWCNT and the metallopolymer-SWCNT composites at f_C = 90% are summarized in Table 1.

Table 1. TE properties of the composites at f_C = 90% and the neat SWCNT.

Polymer component	σ (S·m^{-1})	*S* (μV·K^{-1})	*PF* (μW·m^{-1}·K^{-2})
P1-SWCNT	7.90 × 10^4	27.4	59.5
P1-CoCl$_2$-SWCNT	7.80 × 10^4	23.8	44.1
P1-NiCl$_2$-SWCNT	9.25 × 10^4	27.7	71.0
P1-CuCl$_2$-SWCNT	6.66 × 10^4	24.8	40.9
P2-SWCNT	5.71 × 10^4	24.7	35.0
P2-CoCl$_2$-SWCNT	5.34 × 10^4	25.7	35.4
P2-NiCl$_2$-SWCNT	4.47 × 10^4	26.5	31.3
P2-CuCl$_2$-SWCNT	5.73 × 10^4	30.0	50.3
SWCNT	5.33 × 10^4	38.0	77.0

Mechanism exploration

In order to gain more insight on how the linking patterns affect the TE properties of the designed polymers, the band structures of **P1** and **P2** were first studied by solid state UV-Vis diffuse reflectance spectroscopy. For analysis purpose, the reflectance spectra (Figure 6a) were converted to the plots showing the correlation between Kubelka-Munk function and photon energy *hv* (Figures 6b and 6c) so as to determine the band gaps of these two polymers. Clearly, the energy gaps of **P1** and **P2** were 2.10 and 2.59 eV, respectively, implying that **P1** exerted a narrower energy gap between the Fermi level and the top of the valence band and thus required a lower activation energy.

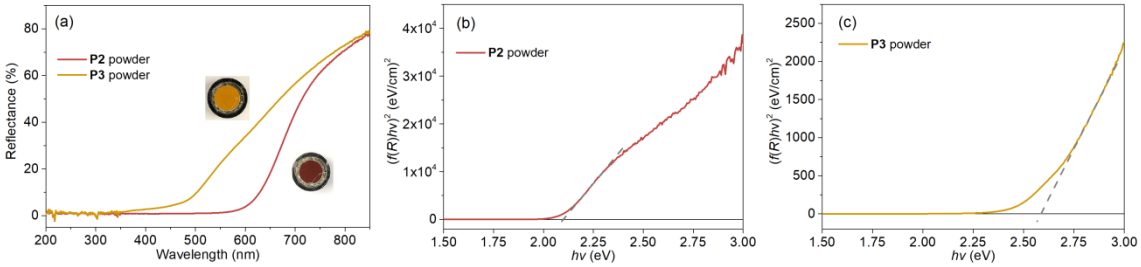

Figure 6. (a) UV-Vis diffuse reflectance spectra of neat **P1** and **P2** powders. (b) The corresponding Kubelka-Munk function versus energy plots of **P1** and (c) **P2** powder. Insets: pictures of **P1** (red) and **P2** (dark yellow) powders taken under daylight.

Further research was conducted on the molecular level where the simplified version of **P1** and **P2** was designed, synthesized and labelled as model compounds **MC-1** and **MC-2** accordingly (Figures 7a and 7b). Their UV-Vis absorption spectra (Figure S6) displayed the absorption maxima at 397 and 378 nm in THF, revealing the energy gaps of 2.62 eV and 2.77 eV for **MC-1** and **MC-2**, respectively. This result confirmed that with the same molecular fragment, the C=C-linked molecule possessed a better conjugation than the C≡C-featured version. Deeper investigations were conducted by carrying out density functional theory calculations on 6-31G* basis set. As illustrated in Figs. 8c and 8d, two phenyl rings on the identical side of the di-imine moiety adopted a coplanar arrangement in both compounds. It is worth noting that, for **MC-1** specifically, the coplanar property was extended to all phenyl rings within one imine molecule, which allowed for better conjugation and higher electrical conductivity. By comparison, in molecule **MC-2**, a twisted structure with a dihedral angle of about 80° between planes P_1P_2 and P_3P_4 was observed, which reduced the conjugation to a large extent. As a consequence, in the polymerized systems **P1** and **P2**, we inferred that such an effect induced by the conformational difference would probably be amplified. In **P1**, each segment possessed almost the same plane as its adjacent ones, rendering the entire polymer chain a quasi-planar geometry. In the aggregated state, such a structure was in favour of establishing more efficient intramolecular interactions between the polymer molecules and SWCNT by setting the planes lying on the SWCNT surfaces (Figure S7a). Particularly, at the high SWCNT doping ratio, **P1** particles were dispersed more thoroughly and coated on the SWCNT network more uniformly, leading to a superior charge carrier migration system in the in-plane, through-plane and polymer-SWCNT fashions and thus better TE properties. However, in **P2**-SWCNT, there may be a considerable number of polymer segments standing on the SWCNT surfaces (Figure S7b), which enlarged the contact distance and resulted in lowered TE properties.

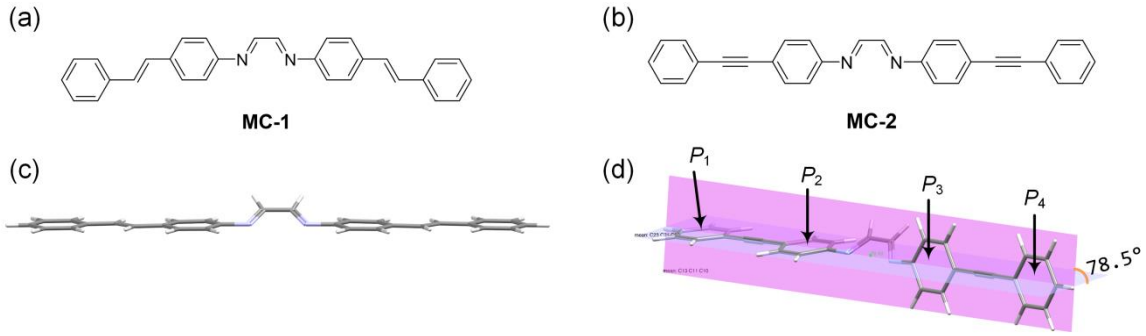

Figure 7. Molecular structures of (a) **MC-1** and (b) **MC-2**. The optimized molecular conformations of (c) **MC-1** and (d) **MC-2**. Note that the phenyl rings P_1 and P_2 are in the light purple plane, while phenyl rings P_3 and P_4 share the same magenta plane.

Conclusion

In conclusion, two types of conducting polymers were designed, synthesized and blended with SWCNTs to assess how the linking groups of the polymer segments, viz. C=C and C≡C units, exerted influence on the TE properties. Morphology studies revealed that a dense and uniform thin film with perfectly dispersed polymer particles was in favour of yielding higher TE performance. With the increase of the SWCNT doping ratio, the electrical conductivities of all the composites were remarkably boosted, but the Seebeck coefficients almost retained the original levels. By coordinating with transition metal ions, the TE performances were readily tuned. Interestingly, most **P1**-SWCNT, **P1-$CoCl_2$**-SWCNT and **P1-$NiCl_2$**-SWCNT composites gave higher *PF* values when compared with their triple bond versions at high doping ratios exceeding 45%. Spectroscopic analysis suggested that **P1** was of narrower band gap than **P2**, which provided favourable condition to yield higher electrical conductivity. Further research on the model compounds indicated that **MC-1** adopted an almost planar conformation, while **MC-2** preferred a highly twisted geometry. Such structural difference may affect the contact mode with SWCNT networks and thus becomes the key reasons that bring about the significant distinction in the extent of conjugation, band gap and

TE properties. We believe this work provides a valuable reference for the structural design of metallopolymer-based OTE materials, and will thus speed up the future work of this field effectively.

Experimental Section

Materials

39% Glyoxal aqueous solution, $NiCl_2$ and 1,2-dichloroethane were purchased from TCI. Anhydrous $CoCl_2$ and $CuCl_2$ were purchased from Acros Organics. SWCNTs (diameter: 1-2 nm, length: 5-30 μm, purity > 95%) were purchased from XFNANO. Other chemicals were purchased from Energy Chemical and used as received.

Preparation of poly(Schiff base)s P1 and P2

The detailed synthetic routes are summarized in Fig. S1. As a general protocol, under a nitrogen atmosphere, 2.0 mmol arylamine **1** or **2** (Scheme 1) was dissolved in a minimum amount of CH_2Cl_2 and the resulting solution was diluted with 8 mL ethanol. Then 0.27 mL 39% glyoxal was injected slowly. The resulting suspension was stirred at room temperature (RT) overnight. After that, the precipitate was collected by filtration and was washed repeatedly with CH_2Cl_2 and ethanol until the dropping filtrate became colourless. Pure polymers **P1** and **P2** were obtained as a dark red powder and a dark yellow powder, respectively, after drying under reduced pressure.

Preparation of the metallated poly(Schiff base)s P1-MCl_2 and P2-MCl_2

In a glass vial, 23 mg poly(Schiff base) was thoroughly dispersed in a mixture of 10 mL methanol and 5 mL THF by sonication. Then a solution of 13 mg MCl_2 (M = Co, Ni and Cu) in 4 mL methanol was added in a dropwise manner with vigorous stirring. The reaction was maintained at RT for 1 day. Finally, the solid was isolated, washed with copious methanol and dried *in vacuo*, yielding the metallated products.

Preparation of the metallopolymer-SWCNT composite films

In a round bottom flask, 100 mg SWCNT was added to 100 mL 1,2-dichloroethane. The mixture was cooled with an ice bath and fully dispersed in an ultrasonic homogenizer at a power of 95 W for 90 min. Then 1.0 mL of the formed dispersion was transferred to a glass vial containing the polymers and the vial was sonicated at 0 °C for 2 h. The dosage of the polymer depends on the doping ratio. The resulting gel-like mixtures were added to clean glass substrates in a dropwise manner until the substrates were fully covered, and the thin films would be ready for subsequent characterizations after solvent evaporation. The abovementioned doping method could eliminate the undesired effects resulting from the soluble impurities adsorbed by SWCNTs including residual reactants, soluble oligomers or free metal ions. The length and the width of the as-prepared films were both 15 mm and the thickness was measured on a Bruker DektakXT surface profiler with a diamond-tipped stylus whose radius was 2.5 μm.

Experimental condition of TE tests

The electrical conductivities and Seebeck coefficients of the prepared films were measured on a JouleYacht MRS-3RT TE Testing System (System) at RT. The System was calibrated with the standard nickel ribbon provided by the manufacturer. The composites were loaded to the dark sample chamber where light was avoided. The electrical conductivity was measured with the four-point method. As for the acquisitions of Seebeck coefficient, an increasing temperature gradient was formed across the thin film where one thermocouple kept the cold end of the sample at ca. RT and the other one gradually heated the composite up. Upon heating, the voltage potential was recorded in real time. The entire process was controlled automatically by the software and the highest temperature was confined to below 60 °C. After completion of the measurement, the film was allowed to cool to RT naturally before the next trial.

Acknowledgements

We would like to acknowledge the financial support from the Science, Technology and Innovation Committee of Shenzhen Municipality (JCYJ20180507183413211), the National Natural Science Foundation of China (51873176 and 21905241), Hong Kong Research Grants Council (PolyU123384/16P), the Hong Kong Polytechnic University (1-ZEIC), Research Institute for Smart Energy (CDA2) and Ms. Clarea Au for the Endowed Professorship in Energy (847S).

Conflict of interest

The authors declare no conflict of interest.

Keywords: thermoelectric • polymer linker • metallopolymer • single-walled carbon nanotube • composite

[1] a) A. Shakouri, *Ann. Rev. Mater. Res.* **2011**, *41*, 399-431; b) H. E. Katz, T. O. Poehler, *Innovative Thermoelectric Materials*, Imperial College Press, Singapore, **2016**; c) Z. Sun, J. Li, W. Y. Wong, *Macromol. Chem. Phys.* **2020**, *221*, 2000115.

[2] a) Z. Tang, L. Hu, T. Zhu, X. Liu, X. Zhao, *J. Mater. Chem. C* **2015**, *3*, 10597-10603; b) L. Hu, T. Zhu, X. Liu, X. Zhao, *Adv. Funct. Mater.* **2014**, *24*, 5211-5218; c) B. Zhu, X. Liu, Q. Wang, Y. Qiu, Z. Shu, Z. Guo, Y. Tong, J. Cui, M. Gu, J. He, *Energy Environ. Sci.* **2020**, *13*, 2106-2114.

[3] a) Q. Zhang, H. Wang, W. Liu, H. Wang, B. Yu, Q. Zhang, Z. Tian, G. Ni, S. Lee, K. Esfarjani, G. Chen, Z. Ren, *Energy Environ. Sci.* **2012**, *5*, 5246-5251; b) L. You, Y. Liu, X. Li, P. Nan, B. Ge, Y. Jiang, P. Luo, S. Pan, Y. Pei, W. Zhang, G. J. Snyder, J. Yang, J. Zhang, J. Luo, *Energy Environ. Sci.* **2018**, *11*, 1848-1858; c) S. A. Yamini, H. Wang, Z. M. Gibbs, Y. Pei, S. X. Dou, G. J. Snyder, *Phys. Chem. Chem. Phys.* **2014**, *16*, 1835-1840.

[4] a) R. Basu, S. Bhattacharya, R. Bhatt, M. Roy, S. Ahmad, A. Singh, M. Navaneethan, Y. Hayakawa, D. K. Aswal, S. K. Gupta, *J. Mater. Chem. A* **2014**, *2*, 6922–6930; b) S. Bathula, M. Jayasimhadri, B. Gahtori, N. K. Singh, K. Tyagi, A. K. Srivastava, A. Dhar, *Nanoscale* **2015**, *7*, 12474-12483.

[5] a) Q. Zhang, Y. Sun, W. Xu, D. Zhu, *Adv. Mater.* **2014**, *26*, 6829-6851; b) G. Chen, W. Xu, D. Zhu, *J. Mater. Chem. C* **2017**, *5*, 4350-4360; c) R. Kroon, D. A. Mengistie, D. Kiefer, J. Hynynen, J. D. Ryan, L. Yu, C. Muller, *Chem. Soc. Rev.* **2016**, *45*, 6147-6164.

[6] J. T. Li, T. Lei, *Chem. Asian J.* **2021**, *16*. DOI: 10.1002/asia.202100285.

[7] a) B. Russ, A. Glaudell, J. J. Urban, M. L. Chabinyc, R. A. Segalman, *Nat. Rev. Mater.* **2016**, *1*, 1-14; b) H. Wang, C. Yu, *Joule* **2019**, *3*, 53-80.

[8] M. Lindorf, K. A. Mazzio, J. Pflaum, K. Nielsch, W. Brütting, M. Albrecht, *J. Mater. Chem. A* **2020**, *8*, 7495-7507.

[9] a) M. H. Jeong, A. Sanger, S. B. Kang, Y. S. Jung, I. S. Oh, J. W. Yoo, G. H. Kim, K. J. Choi, *J. Mater. Chem. A* **2018**, *6*, 15621-15629; b) T. G. Novak, H. Shin, J. Kim, K. Kim, A. Azam, C. V. Nguyen, S. H. Park, J. Y. Song, S. Jeon, *ACS Appl. Mater. Interfaces* **2018**, *10*, 17957-17962; c) Z. Fan, J. Ouyang, *Adv. Electron. Mater.* **2019**, *5*, 1800769.

[10] a) C. T. Hong, Y. Yoo, Y. H. Kang, J. Ryu, S. Y. Cho, K.-S. Jang, *RSC Adv.* **2015**, *5*, 11385-11391; b) S. Qu, Q. Yao, L. Wang, Z. Chen, K. Xu, H. Zeng, W. Shi, T. Zhang, C. Uher, L. Chen, *NPG Asia Mater.* **2016**, *8*, e292; c) S. Mardi, M. Pea, A. Notargiacomo, N. Yaghoobi Nia, A. Di Carlo, A. Reale, *Materials (Basel)* **2020**, *13*, 1404.

[11] a) Y. Sun, P. Sheng, C. Di, F. Jiao, W. Xu, D. Qiu, D. Zhu, *Adv. Mater.* **2012**, *24*, 932-937; b) Y. Cui, J. Yan, Y. Sun, Y. Zou, Y. Sun, W. Xu, D. Zhu, *Sci. Bull.* **2018**, *63*, 814-816; c) W. Shi, G. Wu, K. Hippalgaonkar, J. S. Wang, J. Xu, S. W. Yang, *J. Am. Chem. Soc.* **2018**, *140*, 13200-13204.

[12] L. Wang, C. Pan, Z. Chen, W. Zhou, C. Gao, L. Wang, *ACS Appl. Energy Mater.* **2018**, *1*, 5075-5082.

[13] a) O. Bubnova, X. Crispin, *Energy Environ. Sci.* **2012**, *5*, 9345–9362; b) Q. Zhang, Y. Sun, W. Xu, D. Zhu, *Energy Environ. Sci.* **2012**, *5*, 9639–9644; c) G. Wu, Y. Xue, L. Wang, X. Wang, G. Chen, *J. Mater. Chem. A* **2018**, *6*, 3376-3380; d) I. H. Jung, C. T. Hong, U. H. Lee, Y. H. Kang, K. S. Jang, S. Y. Cho, *Sci. Rep.* **2017**, *7*, 44704.

[14] a) Y. Zhou, Y. Liu, X. Zhou, Y. Gao, C. Gao, L. Wang, *J. Power Sources* **2019**, *423*, 152-158; b) Y. Zhou, X. Yin, Y. Liu, X. Zhou, T. Wan, S. Wang, C. Gao, L. Wang, *ACS Sustainable Chem. Eng.* **2019**, *7*, 11832-11840; c) C. J. An, Y. H. Kang, H. Song, Y. Jeong, S. Y. Cho, *J. Mater. Chem. A* **2017**, *5*, 15631-15639; d) J. Jung, E. H. Suh, Y. J. Jeong, H. S. Yang, T. Lee, J. Jang, *ACS Appl. Mater. Interfaces* **2019**, *11*, 47330-47339; e) J. Y. Kim, J. H. Mo, Y. H. Kang, S. Y. Cho, K. S. Jang, *Nanoscale* **2018**, *10*, 19766-19773; f) Y. Zhang, Q. Zhang, G. Chen, *Carbon Energy* **2020**, *2*, 408-436.

[15] L. Liang, C. Gao, G. Chen, C.-Y. Guo, *J. Mater. Chem. C* **2016**, *4*, 526-532.

[16] C. Gao, G. Chen, *J. Mater. Chem. A* **2016**, *4*, 11299-11306.

[17] S. A. Gregory, A. K. Menon, S. Ye, D. S. Seferos, J. R. Reynolds, S. K. Yee, *Adv. Energy Mater.* **2018**, *8*, 1802419.

[18] L. Wang, C. Pan, A. Liang, X. Zhou, W. Zhou, T. Wan, L. Wang, *Polym. Chem.* **2017**, *8*, 4644-4650.

[19] a) V. Vijayakumar, E. Zaborova, L. Biniek, H. Zeng, L. Herrmann, A. Carvalho, O. Boyron, N. Leclerc, M. Brinkmann, *ACS Appl. Mater. Interfaces* **2019**, *11*, 4942-4953; b) C. K. Mai, R. A. Schlitz, G. M. Su, D. Spitzer, X. Wang, S. L. Fronk, D. G. Cahill, M. L. Chabinyc, G. C. Bazan, *J. Am. Chem. Soc.* **2014**, *136*, 13478-13481.

[20] P. J. Larkin, in *Infrared and Raman Spectroscopy*, 2nd ed., Elsevier, United States, **2018**, pp. 85-134.

[21] a) G. Bepete, K. S. Coleman, in *Comprehensive Nanoscience and Nanotechnology, Vol. 1* (Eds.: D. L. Andrews, R. H. Lipson, T. Nann), Academic Press, **2019**, pp. 205-218; b) S. Nanot, N. A. Thompson, J.-H. Kim, X. Wang, W. D. Rice, E. H. Hároz, Y. Ganesan, C. L. Pint, J. Kono, in *Springer Handbook of Nanomaterials* (Ed.: R. Vajtai), Springer, Berlin, **2013**, pp. 105-146.

[22] D. R. Samarajeewa, G. R. Dieckmann, S. O. Nielsen, I. H. Musselman, *Carbon* **2013**, *57*, 88-98.

[23] a) M. T. Nguyen, R. A. Jones, B. J. Holliday, *Macromolecules* **2017**, *50*, 872-883; b) B. J. Holliday, T. M. Swager, *Chem. Commun.* **2005**, 23-36.

[24] C. Meng, C. Liu, S. Fan, *Adv. Mater.* **2010**, *22*, 535-539.